REVIEW ARTICLE

Instrumentation for low-energy electron diffraction

M. G. Lagally and J. A. Martin

Department of Metallurgical and Mineral Engineering and Materials Science Center, University of Wisconsin-Madison, Madison, Wisconsin 53706

(Received 11 November 1982; accepted 26 June 1983)

Recent developments in instrumentation for low-energy electron diffraction (LEED) are reviewed. After a summary of the major types of measurements in LEED, the properties of LEED instruments that are important in performing these measurements are described. A detailed discussion is presented on the major components of a LEED diffractometer. LEED is compared briefly to some other techniques that are sensitive to surface structure.

PACS numbers: 07.80. + x, 61.14.Hg

INTRODUCTION

Since the advent of ultrahigh vacuum systems, about 30 years ago, which made reliably clean surfaces possible, surface crystallography studies have played a major and increasingly important role in the understanding of chemical, electronic, and transport properties of surfaces. A number of techniques exist that provide surface structural information. Certainly the oldest and best developed of these is low-energy electron diffraction (LEED). Beginning with the discovery of electron diffraction by Davisson and Germer[1] in 1927, there has been a continuing level of activity of increasing intensity. Several major advances in instrumentation were made along the way. These are well known and include the instruments of Sproull,[2] Ehrenberg,[3] Lander *et al.*,[4] Caldwell,[5] and Park and Farnsworth.[6] These instruments, and modifications thereof, have been used (some in only specialized ways) for one or more of the types of studies that a surface crystallography technique is in principle capable of, namely the determination of unit mesh shapes and sizes, the determination of surface atom equilibrium positions, the investigation of the thermodynamics and kinetics of ordering in surfaces and overlayers, and the investigation of structural defects of various kinds.[7] As a consequence of the recognition that instruments with greater sensitivity, speed, or resolving power were becoming necessary to address surface structural problems with the same precision that is being obtained in surface chemical and electronic measurements, a number of improvements in LEED instrumentation have been made in recent years. These are discussed in this paper. In this section we give a brief review of diffraction theory, with the purpose of putting into perspective the measurements that are required to obtain particular structural information. In the second section the questions of measurement precision and the sensitivity and resolving power of a LEED instrument will be briefly addressed. This is followed by a detailed description of the criteria for design and operation of the main components of a LEED diffractometer: the electron gun, the detector, and the sample goniometer. We end with a brief comparison of LEED to other techniques giving surface structural information and with some speculations on future developments in LEED instrumentation.

The ideal probe of the geometric structure of an object is radiation with wavelength of the order of the dimensions one is trying to resolve. Such radiation is diffracted by the periodic arrangement of scatterers in the object. If one considers the elastic scattering of radiation with momentum $\mathbf{k}_0$ from a rigid cubic crystal with lattice points

$$\mathbf{r}_j = m_1\mathbf{a} + m_2\mathbf{b} + m_3\mathbf{c}\,, \tag{1}$$

where m_1, m_2, and m_3 are integers, with atoms located within each unit cell at positions

$$\boldsymbol{\rho}_n = u_n\mathbf{a} + v_n\mathbf{b} + w_n\mathbf{c}\,, \tag{2}$$

where u_n, v_n, and w_n are fractions, the amplitude at a given momentum transfer $\mathbf{S} = \mathbf{k} - \mathbf{k}_0$ is given by

$$A(\mathbf{S}) = \sum_{j,n} f_n(\theta, E)\exp[i\mathbf{S}\cdot(\mathbf{r}_j + \boldsymbol{\rho}_n)]\,. \tag{3}$$

The sum is over lattice sites j and the atoms n within a unit cell. $f_n(\theta, E)$ is the atomic scattering factor of the nth atom, where θ is half the scattering angle and E is the energy of the radiation. Separating the sums,

$$A(\mathbf{S}) = F(\theta, E)\sum_j \exp[i(\mathbf{S}\cdot\mathbf{r}_j)]\,, \tag{4}$$

where

$$F(\theta, E) = \sum_n f_n(\theta, E)\exp[i\mathbf{S}\cdot\boldsymbol{\rho}_n] \tag{5}$$

is the structure factor. The intensity in the kinematic approximation then is

$$I(\mathbf{S}) = A(\mathbf{S})A^*(\mathbf{S}) = F(\theta, E)^2\mathscr{I}(\mathbf{S})\,, \tag{6}$$

where $\mathscr{I}(\mathbf{S})$ is called the interference function. $\mathscr{I}(\mathbf{S})$ can be visualized using the concept of the reciprocal lattice. For a three-dimensional infinite crystal, the reciprocal lattice is a three-dimensional array of points whose positions with respect to an arbitrary origin are given by the vectors $\mathbf{G}_{hkl}$, where $|\mathbf{G}_{hkl}| = n2\pi/d_{hkl}$ and d_{hkl} is the distance between (hkl) planes. The interference function is periodic with $\mathbf{G}_{hkl}$, and for an arbitrary momentum transfer, $\mathbf{S}$ can be written in terms of $\mathbf{G}_{hkl}$ and the deviation parameter $\mathbf{s} = \mathbf{S} - \mathbf{G}_{hkl}$. For a crystal with dimensions N_1a, N_2b, and N_3c, where a, b, and c are the lattice constants,

$$\mathscr{I}(\mathbf{G}_{hkl} + \mathbf{s}) = \frac{\sin^2 \frac{1}{2}N_1(\mathbf{G}_{hkl} + \mathbf{s})\cdot\mathbf{a}}{\sin^2 \frac{1}{2}(\mathbf{G}_{hkl} + \mathbf{s})\cdot\mathbf{a}}\,\frac{\sin^2 \frac{1}{2}N_2(\mathbf{G}_{hkl} + \mathbf{s})\cdot\mathbf{b}}{\sin^2 \frac{1}{2}(\mathbf{G}_{hkl} + \mathbf{s})\cdot\mathbf{b}} \times\frac{\sin^2 \frac{1}{2}N_3(\mathbf{G}_{hkl} + \mathbf{s})\cdot\mathbf{c}}{\sin^2 \frac{1}{2}(\mathbf{G}_{hkl} + \mathbf{s})\cdot\mathbf{c}}\,. \tag{7}$$

 © 1983 American Institute of Physics

Downloaded 05 Apr 2007 to 128.104.198.190. Redistribution subject to AIP license or copyright, see http://rsi.aip.org/rsi/copyright.jsp

$\mathscr{I}(\mathbf{G}_{hkl}+\mathbf{s})$ has its maximum value, $\mathscr{I}(\mathbf{G}_{hkl})$, when $\mathbf{s}=0$, i.e., when $\mathbf{S}$ satisfies the Laue conditions

$$\mathbf{S}=\mathbf{G}_{hkl} \tag{8}$$

or

$$\mathbf{S}\cdot\mathbf{a}=2\pi h\,,\quad \mathbf{S}\cdot\mathbf{b}=2\pi k\,,\quad \mathbf{S}\cdot\mathbf{c}=2\pi l\,,$$

where h, k, and l are integers. The maxima in the interference function have heights proportional to $(N_1N_2N_3)^2$ and widths in three orthogonal directions in $\mathbf{S}$ space proportional to $1/N_1a$, $1/N_2b$, and $1/N_3c$.

For an adsorbed monolayer (or in any case where a phase is only one atomic layer thick) it is easy to demonstrate that the reciprocal lattice becomes a set of rods normal to the plane of the layer. In Eq. (7), $N_3=1$ and the third term equals one, implying that the interference function has a constant value for all values of $(\mathbf{G}_{hkl}+\mathbf{s})\cdot\mathbf{c}$. Intermediate between this limit and that of an infinite three-dimensional crystal is a crystal that has finite dimension in the third direction. This situation is approximated for an infinite three-dimensional crystal if the radiation used for the diffraction experiment does not penetrate the sample to a great depth. Low-energy electrons have cross sections for both elastic and inelastic scattering that are quite large (each of the order of several Å^2), which limit their penetration to several atomic planes. This causes a modulation in the interference function in the corresponding (N_3) direction in reciprocal space. Because the interference function never goes to zero in this direction, it is customary to describe the reciprocal lattice as a set of rods, as for a single layer.

A generally useful representation of diffraction from a lattice is in terms of its reciprocal lattice and the Ewald construction. The Ewald sphere gives simply the conservation of energy for elastic scattering, i.e., $\lambda_{\text{in}}=\lambda_{\text{out}}$ or $|\mathbf{k}_0|=|\mathbf{k}|$, where λ and $\mathbf{k}$ are, respectively, the electron wavelength and momentum. The superposition of the Ewald sphere onto the reciprocal lattice shows conservation of momentum as well as energy, in the form of the Laue conditions $\mathbf{S}=\mathbf{G}_{hkl}$. The diffracted-intensity distribution in angle at constant energy, or diffraction pattern, is given by the intersection of the Ewald sphere with the reciprocal lattice. This simplest of all diffraction measurements is illustrated in Fig. 1(a) in real and reciprocal space.

The interference of amplitude scattered from the several layers illuminated by a beam of low-energy electrons forms the basis of probably the most important, and certainly the most common, measurement in LEED, the integrated intensity versus energy profile (commonly called an I vs E curve but more properly identified as a $\int_{\text{detector}} J_{hk}(\vartheta,E)d\Omega$ vs E curve). From it the equilibrium positions of surface atoms can be determined by comparison to model calculations.[8] For this type of measurement, the intensity in a reflection, $J_{hk}(\vartheta,E)$, integrated over the solid angle of the detector, $d\Omega$, is determined as a function of incident-beam energy, effectively scanning the reciprocal lattice in $G_\perp$, the component of a reciprocal-lattice vector normal to the surface, at fixed $\mathbf{G}_\|$, the component parallel to the surface. This is illustrated in real and reciprocal space in Fig. 1(b). ϑ is the colatitude angle measured from the surface normal. The *sensitivity* of a LEED diffractometer is the feature of major importance in this measurement. Frequently this is simply because some peaks in the diffracted intensity (e.g., from fractional monolayers) are small. In other cases electron-beam damage to the overlayer or surface structure requires use of as low a total dose as possible. Often, however, the need for sensitivity implies only a need for speed in data acquisition, because a large data base is required for accurate analysis of the equilibrium positions, and because the LEED intensity is usually quite sensitive to surface contamination.

So far, it has been assumed that the crystal surface is infinite, perfect, and rigid. In this case, the reciprocal-lattice rods will have zero width and the diffraction spots will be sharp. In the presence of defects the reciprocal-lattice rods have a finite width, which manifests itself as a broadening of the diffracted-beam angular profiles. This can readily be seen from Eq. (7) by letting N_1 or N_2 be finite, in which case the corresponding terms are no longer delta functions. In order to determine finite-size effects in surfaces, the angular distribution of intensity in a given reflection must be measured, i.e., the differential intensity must be measured as a function of $\mathbf{G}_\|$ at constant $G_\perp$. Three ways to do this are illustrated in real and reciprocal space in Figs. 1(c)–1(e).

Different types of surface defects can cause different broadening of the intensity distribution, and this fact can be used, as in x-ray diffraction,[9] to distinguish and quantify defects.[10] Reciprocal lattices for some surface or adsorbed-layer defects that can presently be analyzed by consideration of the dependence of the LEED angular profile on diffraction variables are illustrated in Fig. 2. It is apparent that an instrument with a high *resolving power*, i.e., the ability to differentiate between two signals lying close in angle, is a prerequisite for identifying such defects. A high resolving power implies the ability to resolve defects that lie far apart on the surface, i.e., the ability to observe large ordered regions and to determine their sizes. A low resolving power, conversely, implies that a surface with a high structural-defect density cannot be distinguished from one that is perfect. The resolving power of a diffractometer is related to the diffractometer response and the measurement accuracy.[11,12]

In Sec. I we briefly consider the sensitivity and resolving power of LEED diffractometers in the context of measurement precision.

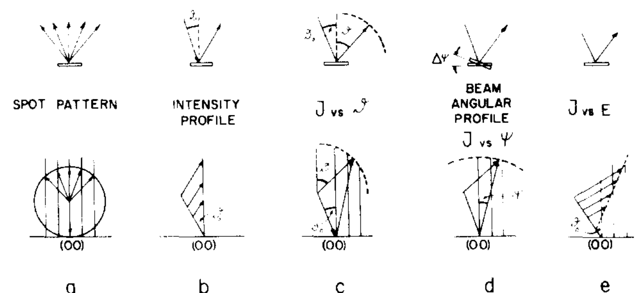

FIG. 1. LEED measurements illustrated in real and reciprocal space. (a) Display of the diffraction pattern; (b) measurement of intensity versus energy profiles; (c) measurement of angular profiles by rotating the detector; (d) measurement of angular profiles by tilting the sample; (e) measurement of angular profiles by varying the incident-beam energy. Note that (c), (d), and (e) give different cuts across a reciprocal-lattice rod.

Downloaded 05 Apr 2007 to 128.104.198.190. Redistribution subject to AIP license or copyright, see http://rsi.aip.org/rsi/copyright.jsp

I. LEED INSTRUMENTS AND MEASUREMENT PRECISION

Figure 3 shows schematically the basic elements of a LEED diffractometer: an electron source, a sample goniometer, and a detector for the scattered electrons. An experiment requires the creation of a beam of incident electrons at a fixed energy to use as a probe, and the detection of electrons at the same energy scattered by the surface. In essence one is counting particles and, therefore, the ratio of the true signal current and the noise current can be described by the well-known relationship between signal and shot noise,[13]

$$\frac{J_{\text{true}}}{J_{\text{shot noise}}} \propto (\sigma i t)^{1/2}, \qquad (9)$$

where i is the incident current, t is the time of measurement, and σ is the probability of measuring a diffracted electron for each incident electron. σ can, therefore, be identified with the sensitivity. It includes both physical factors, such as scattering powers and the inelastic-scattering cross section, and instrumental factors, such as detector size and sensitivity. It is clear from Eq. (9) that the simplest way to increase the signal-to-shot-noise ratio is to increase the dose, i.e., to raise the incident current i or measure for a longer time t. However, as already mentioned, higher doses will lead to greater structural damage in electron-beam-sensitive overlayers or surfaces. The best way to improve the signal-to-shot-noise ratio, within the above constraints, is to increase the sensitivity by increasing σ. This can be most readily accomplished through improved detector efficiency, by increasing collector gain and employing parallel detection schemes, as will be discussed later.

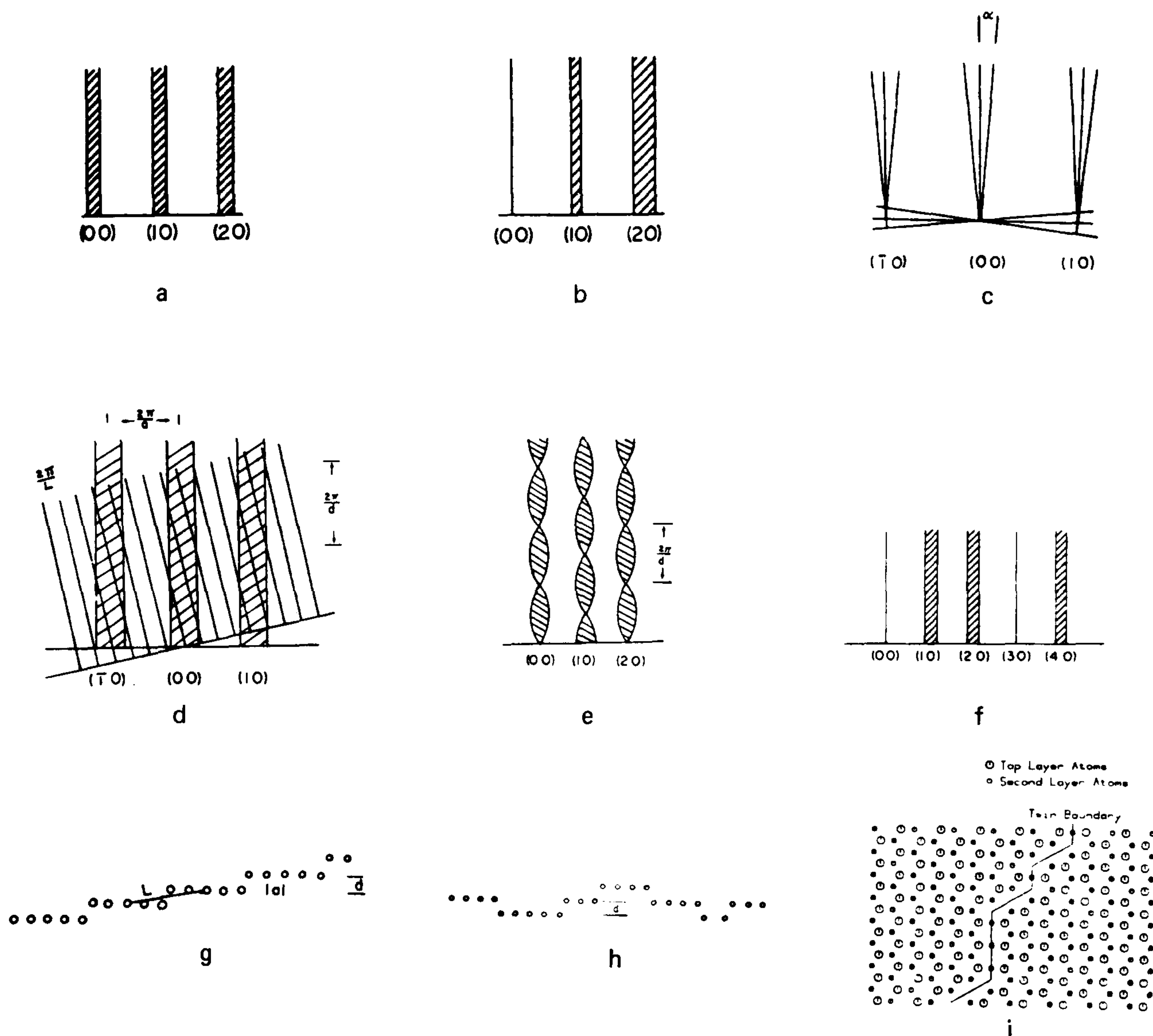

FIG. 2. Schematic diagrams of the influence of various defects on the reciprocal lattice. The shaded region always indicates the full width at half-maximum. In (d), (e), and (f) the real lattice is also shown. (a) Finite-size crystal surfaces; (b) a surface containing inhomogeneous strain; (c) a surface containing large crystallites that are misoriented with respect to each other by a mean angle α, as in a crystal mosaic; (d) a regularly stepped surface with terrace separation L, step height d, and lattice constant a; (e) a surface in which the steps are randomly up or down and the terraces have a random size; (f) a surface or overlayer with translational antiphase boundaries, in this case a (111) surface with twins, where one twin is displaced from the proper position by a third of a lattice constant. The (10) rows run vertically in the schematic of the surface.

Downloaded 05 Apr 2007 to 128.104.198.190. Redistribution subject to AIP license or copyright, see http://rsi.aip.org/rsi/copyright.jsp

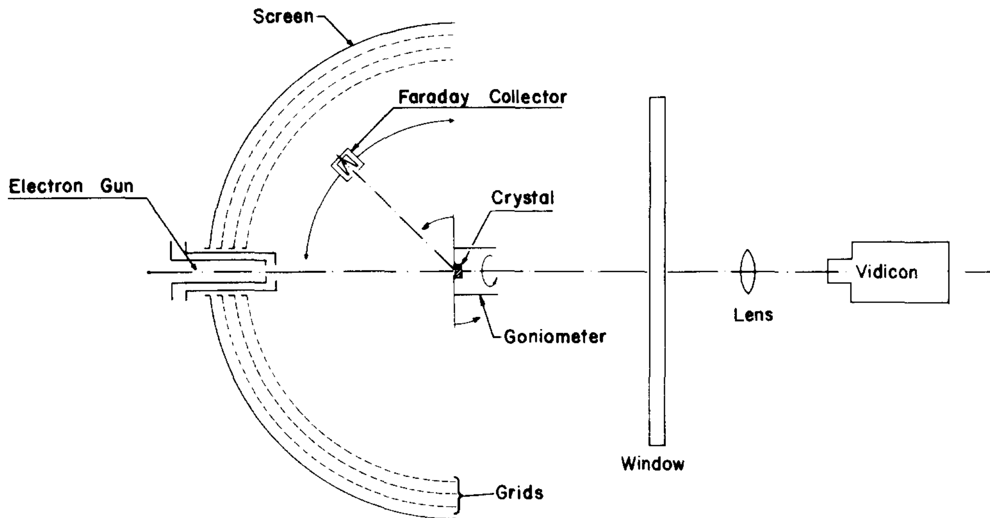

FIG. 3. Schematic view of the basic elements of a low-energy electron diffractometer.

The instrumental factors mentioned above also make a contribution to the broadening of the diffracted beams, i.e., they limit the resolving power. It is possible to quantify this contribution.[12] If $T(\vartheta, E)$ represents the broadening, or instrument response, function,[11] the measured intensity is given by the convolution

$$J(\vartheta, E) = I(\vartheta, E)*T(\vartheta, E),$$

or equivalently

$$J(\mathbf{S}) = I(\mathbf{S})*T(\mathbf{S}). \quad (10)$$

$I(\vartheta, E) \propto I(\mathbf{S})$, the true signal, results from the incoherent sum of diffraction patterns of individual electrons all with the same momentum.[14] $I(\vartheta, E)$ is a delta function if the surface is perfect and a function with some angular spread or "physical width" if the surface is not perfect. $T(\vartheta, E)$ can be thought of as a shape function, whose integral is unity, that distributes the true intensity $I(\vartheta, E)$ over a range of angles in reciprocal space. The major sources of instrumental broadening in diffractometers are the incident-beam divergence or "source extension," γ, of the electron gun, the energy uncertainty in the incident beam, ΔE, the incident-beam diameter D, and the detector aperture width d. As discussed by Park *et al.*,[11] the instrument response function, the distribution in momentum of all the electrons measured by the detector if the sample is perfectly periodic or removed out of the path of the beam, will be

$$T(\vartheta, E) = T(\vartheta, E)_\gamma * T(\vartheta, E)_E * T(\vartheta, E)_D * T(\vartheta, E)_d. \quad (11)$$

The instrument response measured for a typical commercially available LEED instrument has a Gaussian profile near its center, with wings that are more Lorentzian. The importance of the different factors for different LEED diffraction conditions has been discussed.[11,15] The most significant limitation for typical systems operated at commonly used diffraction geometries is the size of the beam at the detector. Because only one beam can be focused on the detector at any time, the beam divergence frequently becomes the real limitation because it contributes to the size of the other diffracted beams.

For angular distribution $[J(\vartheta, E)$ vs $\vartheta]$ measurements, it is important that the instrument response function be narrow and that it be known accurately. This can be quantified by defining a minimum angle of resolution to represent the resolving power of the instrument. If one represents the instrument response function $T(\vartheta, E)$ by a Gaussian with a full width at half-maximum b_T, and the accuracy to which this width is known and to which a measurement of $J(\vartheta, E)$ has been made as $X\,\%$, then the smallest value of the angular width of a signal $I(\vartheta, E)$ that can be resolved by the instrument is[12]

$$\begin{aligned}\vartheta_{\min} &= [(b_T + X\,\%\, b_T)^2 - (b_T - X\,\%\, b_T)^2]^{1/2} \\ &= 2b_T(X\,\%)^{1/2}. \end{aligned} \quad (12)$$

Equation (12) represents the worst possible case for the resolving power of a given instrument, because it is based on extremal values of signal allowed by the error bars. The uncertainty in the measurement, X, is clearly related to the system sensitivity, and thus is a function of the incident-beam current, the detector efficiency, and the measurement time. Values of $\vartheta_{\min}$ for a typical LEED system response and measurement accuracies are 0.2° to 0.5° (depending on the energy). The corresponding resolvable domain sizes are between 200 and 400 Å and are a function of the type of surface defect present.[12] The resolving power can be increased by improving the instrument response (in particular by refining electron gun characteristics) or by improving sensitivity through increased detector efficiency.

Although a high resolving power is not necessary for the integrated-intensity $[\int_{\text{detector}} J_{hk}(\vartheta, E)d\Omega$ vs $E]$ measurements, the instrument response must at least be well known in order to extract reliable data. This can be illustrated as follows. Because LEED instruments in different laboratories commonly have different beam parameters and detector widths, and because intensity versus energy data are usually collected with the detector centered on the maximum intensity rather than by scanning through a reflection, the measured "integrated" intensity $\int_{\text{detector}} J_{hk}(\vartheta, E)d\Omega$ can differ markedly for the same $I_{hk}(\vartheta, E)$ (i.e., for surfaces with identical structures and degrees of order). Thus, for reliable equilibrium position determinations, a knowledge of

Downloaded 05 Apr 2007 to 128.104.198.190. Redistribution subject to AIP license or copyright, see http://rsi.aip.org/rsi/copyright.jsp

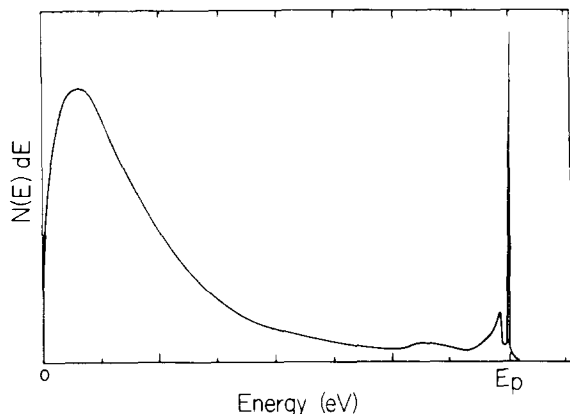

FIG. 4. Schematic energy distribution of secondary electrons emitted from a sample illuminated with an electron beam of energy E_p.

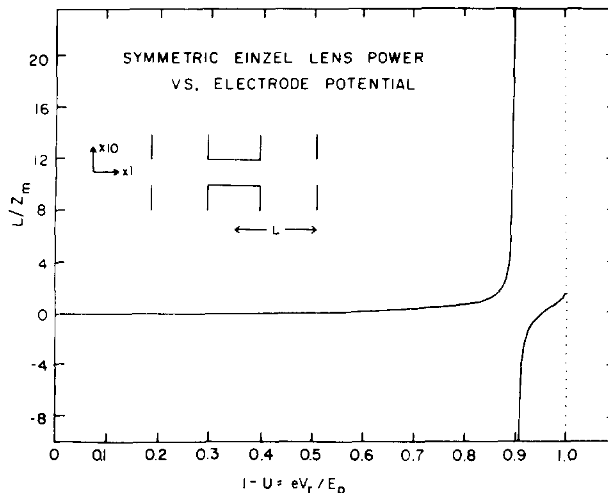

FIG. 5. Dependence of the focal power of a symmetrical unipotential (Einzel) lens with thick central electrode on the ratio of the potentials on the electrodes. The focal power is represented as the reciprocal of the mid-focal length Z_m of the lens in units of L, the distance from the geometric center to the outer electrodes. U is the ratio of the potential at the center of the lens to that of the outer electrodes. In a four-grid retarding-potential analyzer, U corresponds approximately to the ratio of eV_r, the retarding potential on grids No. 2 and No. 3 and E_p, the energy of electrons incident on the grids. The dimensions of the lens shown in the inset are scaled to correspond approximately to the grid aperture size and grid separations in a typical four-grid retarding-potential analyzer (Ref. 17).

$T(\vartheta, E)$ is a necessity to allow an accurate interpretation of the measured intensity.[16]

Several additional experimental parameters not inherent in the simple statistical interpretation of the noise discussed at the beginning of this section can affect the measurement precision. The most important of these are lack of suppression of electrons scattered inelastically from the surface, stray light in some detector schemes, lack of reproducibility in mechanical positioning of the detector or the angle of incidence and position of the beam on the sample, and stray electric or magnetic fields.

The production of inelastic electrons is a consequence of all spectroscopies or techniques in which electrons are emitted. In diffraction, of course, one is interested only in the elastically scattered electrons. As can be seen from Fig. 4, which shows a secondary-electron emission spectrum, the inelastically scattered electrons represent a majority of the electrons emitted from the sample and thus must be suppressed. However, this is not a simple task if one requires at the same time that the angular distribution of elastically scattered electrons not be disturbed. The usual method of suppression of inelastically scattered electrons is with a high-pass filter consisting of a retarding-potential grid in front of the detector. This was illustrated in Fig. 3. The typical arrangement has three grids, with the outer and inner ones at ground and the middle one at negative potential (occasionally four grids are used with the middle two at the same potential for more uniform suppression). This arrangement of grids can, to a good approximation, be represented by an array of thick symmetric Einzel lenses. In order to preserve the angular distribution in passing through this grid structure, the trajectories of electrons with the highest energy (i.e., the elastically scattered electrons) should not be disturbed. The extent that an electron is diverted from its original trajectory in traversing an Einzel lens is described by the lens focal power, given as the ratio of half of the geometric length of the lens to its focal length. Figure 5 shows the focal power of a symmetric Einzel lens as a function of the ratio of retarding voltage on the center electrode and the energy of elastically scattered electrons.[17] It can be seen that the trajectories of the elastically scattered electrons will be significantly affected at retarding potentials greater than about 80% of the energy of these electrons. An experimental verification of this behavior[17] is shown in Fig. 6, where the FWHM of the angular distribution of intensity in a particular LEED reflection is shown as a function of retarding bias on the suppressor grids. The implication of these measurements is that retarding grids must typically be operated at biases that permit a certain fraction of inelastic electrons to enter the detector. The resulting background intensity occurs with all detectors that depend on grids for suppression of inelastically scattered electrons.

Faraday cup detectors exist that do not use grids and effectively suppress inelastically scattered electrons without

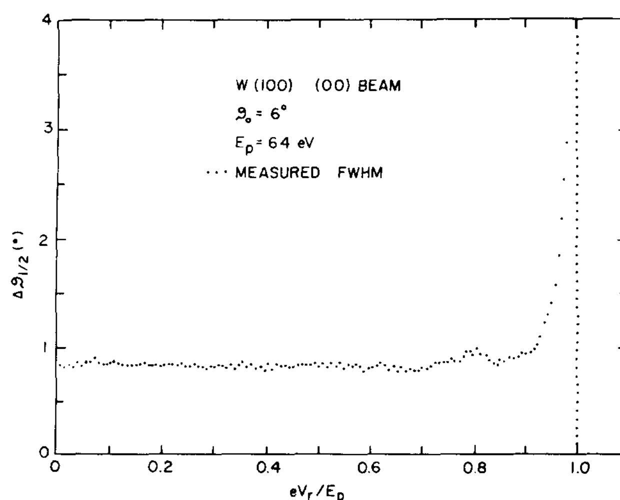

FIG. 6. Full widths at half-maximum of a diffracted beam as a function of retarding potential on the central two grids of a four-grid LEED optics (Ref. 17).

Downloaded 05 Apr 2007 to 128.104.198.190. Redistribution subject to AIP license or copyright, see http://rsi.aip.org/rsi/copyright.jsp

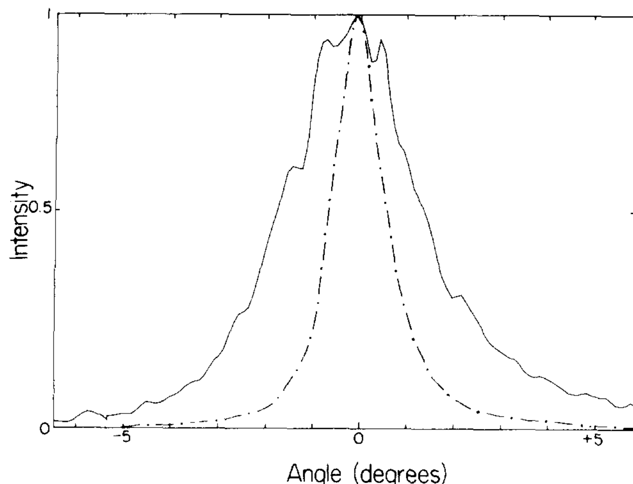

FIG. 7. Comparison of angular profiles of the (01) beam from a sputter-etched and annealed GaAs(110) surface, measured with a grid/fluorescent screen/vidicon detector. Solid curve: annealed at 350 °C for 10 min; dashed curve, annealed at 560 °C for 10 min. Each curve is the average of 30 scans, requiring approximately 1 min. The curves are normalized at their maxima. The actual peak intensities differ by a factor of 7 (Ref. 18).

affecting the angular distribution of elastically scattered electrons. They will be discussed briefly later.

Stray light causes a similar background problem for systems that depend on optical methods of observing the diffraction spot, i.e., whenever a fluorescent screen is used. The magnitude of this background and its angular distribution can be measured by making an intensity scan with the electron beam off or diverted or the screen potential reduced to zero.

Angular distribution $[J(\vartheta, E)$ vs $\vartheta]$ measurements are affected significantly by the inelastic scattering and stray light, because the resulting background intensity may be a large fraction of, or even greater than, the actual signal. The noise is, of course, proportional to the sum of the background and true intensity, and thus the signal-to-noise ratio can become quite small, especially away from the central peak in an angular profile, and as a result the beam shape becomes uncertain. Figure 7 shows typical angular profiles, taken with a vidicon from a fluorescent screen for two surfaces with different structural order,[18] that illustrate the magnitude of this effect.

Intensity versus energy curves $(\int_{\text{detector}} J_{hk}(\vartheta, E) d\Omega$ vs $E)$ are also affected by the above background contributions, but to a lesser degree. Because the measurement is an integral over the detector (which is usually chosen to be large enough to encompass at least the FWHM of the diffracted beam), the background is generally a small fraction of the intensity, except in diffraction features that are themselves very weak. The typical intensity versus energy curve taken with retarding-potential grids consists of peaks sitting on a background that rises with increasing electron beam energy, with the intensities of the small peaks much less certain than those of the large peaks. The magnitude of the background is related to the size of the detector in relation to the size of the Brillouin zone, i.e., in relation to the separation of diffraction spots.

Another contribution to the background intensity is the thermal diffuse scattering.[19] Because of the small energy losses involved, it cannot be discriminated against by any LEED detector. The study of thermal diffuse scattering by LEED is important in its own right; however, in other measurements, it must be dealt with as a background that reduces the measurement precision. It is most easily accounted for by noting differences in angular profiles taken at high and low temperatures, when this is possible.

Uncertainties in detector and incident-beam angles affect the precision in intensity versus energy curves more importantly than background currents. Multiple-scattering contributions to the structure in intensity versus energy profiles[8] make these curves sensitive to changes in angles of incidence of fractions of a degree. Uncertainties in angles of incidence are caused by a lack of repeatability in mechanically setting absolute goniometer positions and also by stray electric and magnetic fields, which affect beam trajectories. Because the instrument response broadens reflections and because the integrated intensity is usually represented by the maximum intensity measured with a fixed-aperture detector, rather than by a scan through the reflection, irreproducibility in setting the detector angle affects intensity versus energy profiles as well.

Angular-profile measurements are less sensitive to angles of incidence because the effects that cause angular broadening are only slowly dependent on $G_{\parallel}$. Absolute detector angles are not important, because the detector must be scanned in any case. However, uncertainty in measuring angular changes, e.g., due to gear backlash in mechanically driven collectors, affects the resolving power.

On the basis of the above discussion, it should be evident where the limitations in LEED instrumentation lie. The two major directions in which development has proceeded are increasing the sensitivity of the detecting system and improving the resolving power by modifications of the electron gun and the detector. A third direction of development has led to greater convenience in operation or in taking particular forms of data. These are discussed in Sec. II.

II. LEED APPARATUS

The major components of a LEED instrument are a gun, a sample goniometer, and a detector, as already shown in Fig. 3. In addition, sample heating or cooling, a gas-handling system or evaporation source, a mass spectrometer, and a separate gun for Auger electron spectroscopy are typically available. In many cases, a LEED diffractometer itself serves as an ancillary tool in UV or x-ray photoelectron or Auger electron spectrometers, or in other surface analysis systems. The focus of the discussion here will be on the gun, goniometer, and detector.

A. Low-energy electron guns

Electron guns used in LEED diffractometers typically have a simple design. They consist of a thermionic cathode, an extraction electrode, an array of focusing electrodes, and electrostatic deflection plates for guiding the beam. A schematic diagram of a commonly used electron gun[20] is shown in Fig. 8. Filaments are usually made of W or thoriated W,

Downloaded 05 Apr 2007 to 128.104.198.190. Redistribution subject to AIP license or copyright, see http://rsi.aip.org/rsi/copyright.jsp

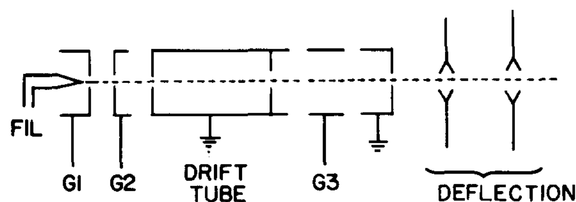

FIG. 8. Schematic diagram of a commonly used low-energy electron gun (Cliftronics model 406S). G_1 is the Wehnelt cylinder and G_2 the extraction anode. The following three elements form an Einzel lens that focuses the beam.

and may be hairpin wires or ribbons. Indirectly heated filaments (oxide, LaB_6, etc.) are also used. In order to avoid background light and contamination of the sample due to evaporation from the filament, some guns have off-axis filaments. The thermionic cathode is situated in a Wehnelt cylinder, a can that completely surrounds the cathode except for the beam extraction aperture. The Wehnelt cylinder can be biased positively or negatively with respect to the cathode, but is typically at about the same potential. Extraction of the beam is achieved with the first electrode of a unipotential lens that then focuses the initially divergent beam. This lens forms an image of the true electron source, which may be part of the hairpin or the aperture of the Wehnelt cylinder, depending on the filament type, the filament current, and the potentials on the Wehnelt cylinder and the extraction electrode. Focal lengths are of the order of 10–30 cm. Such guns have not been optimized with respect to the parameters that give high resolving power. Historically beam currents of 1 μA in a spot of about $\frac{1}{4}$–1-mm diam with a beam divergence of 0.25° to 1° have been considered adequate for LEED.

The beam characteristics of guns of the type shown in Fig. 8 have been tested over a wide range of operating parameters. It is desirable, of course, to achieve maximum intensity with minimum beam diameter and, if possible, zero divergence angle. Beam parameters have been measured with the aid of a simple multiple detector,[21] consisting of three Faraday cups, each with a knife-edge aperture, that are at different distances from the source, as shown in Fig. 9. As each of the three cups is moved into the beam path, the beam profile

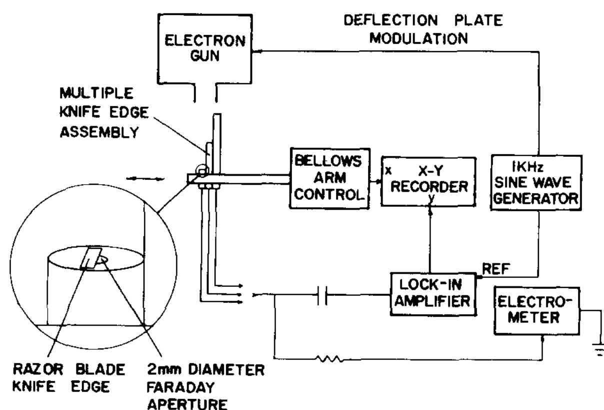

FIG. 9. Schematic diagram of a detector for measuring beam divergence. Several Faraday cups are mounted at different heights. Each cup contains a knife edge across which the beam can be swept. The bellows arm control is used to position each cup in the beam. Comparison of beam diameters at various heights gives the beam divergence (Ref. 21).

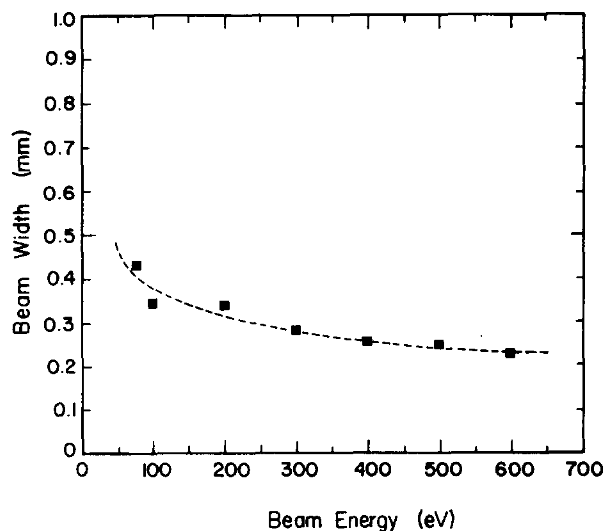

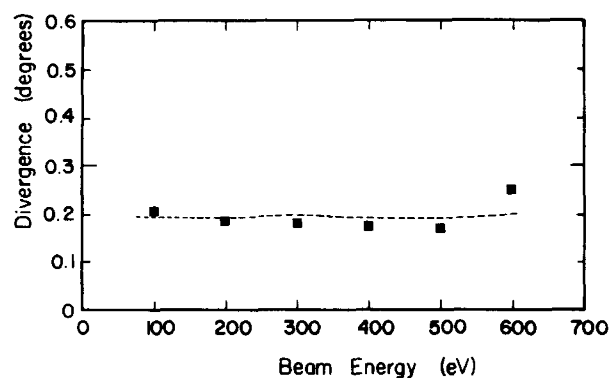

FIG. 10. Properties of low-energy electron guns. The beamwidth and divergence are plotted as a function of energy for a gun with 0.052-in.-diam extraction aperture operated at a beam current of 10^{-7} A and focusing distance of 17 cm (Ref. 22).

can be obtained at the corresponding distance from the sample by rastering the beam across the knife edge. From this measurement the beam diameter D and beam divergence γ can be determined as a function of gun voltage and focusing-electrode potentials. The beam current can be directly measured by each cup. Figure 10 illustrates results typical of these guns.[22] The beam diameter is, in general, a function of the beam energy. The beam diameter can be decreased by reducing Wehnelt cylinder and first-lens element aperture sizes (which are typically about 1 mm in diameter or larger), with consequently greatly reduced beam currents (e.g., 1 nA at 100 eV for a 0.4-mm-diam first-lens aperture). For the 0.1-μA beam currents required with commonly used detector schemes (grids and phosphor screen, or a simple Faraday cup), a minimum beam size of ~200 μm and a minimum divergence of 0.2° appear to be achievable with guns that have the simple designs shown in Fig. 8. Changing the bias on the Wehnelt cylinder with respect to the cathode drastically affects the beam current and its stability with energy, but does not affect the smallest beam diameter achievable for typical current densities (less than 0.2 mA/cm^2). A method that has given stable focusing and uniform beam currents over voltage ranges of several hundred volts is self-biasing of the Wehnelt cylinder with respect to the cathode using a

Downloaded 05 Apr 2007 to 128.104.198.190. Redistribution subject to AIP license or copyright, see http://rsi.aip.org/rsi/copyright.jsp

resistor between the two. A typical value of 570 kΩ gives a small negative bias of the cylinder relative to the cathode. Much larger resistances give too high a negative bias, leading to reduced effective aperture size and much reduced beam currents.

Attempts to improve electrostatic guns include the addition of an extra focusing electrode and optimization of the extraction anode design[22] to reduce beam divergence and beam diameter while maintaining beam currents in the range of 0.1 μA for use with standard detection schemes. An electron gun with electrostatic deflection that will in addition reduce the energy spread in the beam has been designed by Unertl.[23] It incorporates a 127° sector analyzer at the filament to monochromatize the beam before it passes through further focusing and steering electrodes. In typical sector analyzers, a large fraction of the current is lost. Beam currents in this gun will therefore probably be insufficient to use common detectors.

Magnetic focusing is an alternative to electrostatic focusing and has been used in LEED systems since the early days of electron diffraction. Sproull[2] used a simple filament and grid and a magnetic field to separate the specularly diffracted beam from the incident beam. Tucker's modification[24] included an electron gun at 90° to the crystal, rather than simply a filament at 180°, to provide a focused beam. This arrangement has also been used by Dennis and Webb[25] and later by Cohen and Webb,[26] who pointed out that magnetic deflection through 180° provides focusing in the scattering plane, i.e., the instrument response due to beam diameter will be improved in this direction relative to the direction parallel to the magnetic field. Wulfert and Henzler[27] have used the concept of magnetic focusing with a long solenoid to produce the first truly small low-energy beams, with beam sizes of the order of 40 μm in the imaging plane. The magnetic field is along the beam direction. The magnetic field acts as a 1:1 lens that images the crossover of the beam emerging from the Wehnelt cylinder of the gun onto the detector after reflection by the crystal. In such a lens, electrons leaving the source point or object at different angles (or different energies) will return to the axis of the solenoid at different points, causing a smearing of the image. However, this is a negligible effect for a beam with a typical divergence. For a 50-μm beam diameter, the smearing due to a divergence of 1° is less than 1 μm. Because of the small beam currents attainable with this gun, a detector with gain is used, which in Henzler's system[27] is a small-aperture Faraday cup equipped with a channeltron electron multiplier. The minimum angle of resolution for normal incidence for this gun and detector is of the order of $\vartheta_{min} = 0.05°$ (at 50 eV), compared to typical values of $\vartheta_{min} = 0.5°$ in systems with standard guns. The magnetic field focuses electrons of different energies at different points along the field axis. If electrons in only a small range of angles around a given beam are allowed to enter the field, and if the detector aperture is small, the magnetic field provides in principle energy selection against inelastic electrons without the use of grids. A schematic diagram of the gun and detector is shown in Fig. 11.

A recent development in low-energy electron guns is

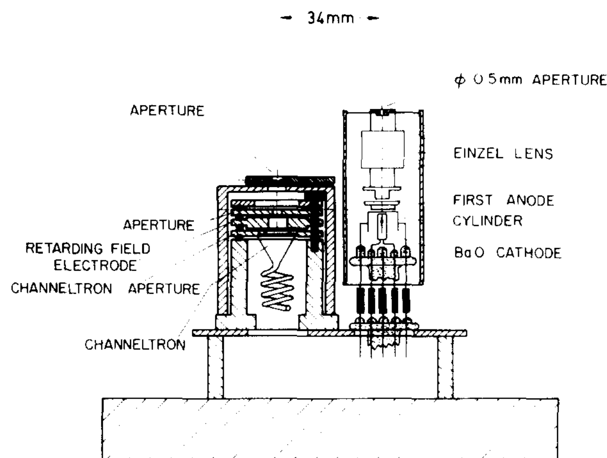

FIG. 11. Configuration of electron gun and detector for a diffractometer with magnetic focusing (Ref. 27).

the use of field emission sources. Field emission sources have been used for some years in high-energy applications, such as scanning and transmission electron microscopes. The major advantage of a field emitter is that it is nearly a point source, in principle making a parallel beam a possibility. This can easily be visualized by considering a point source situated at the focus of a convergent lens. Suitable apertures can then also define a beam with a small diameter. The high luminosity of field emitters makes small beam sizes practical also. A schematic diagram of a typical gun configuration used in high-energy applications is shown in Fig. 12. The extraction geometry consists of an emission tip mounted opposite a ring anode, with several kV extraction potential applied between them. A small portion of the field-emitted current (on the order of 0.1 nA compared to 100-μA emission current)

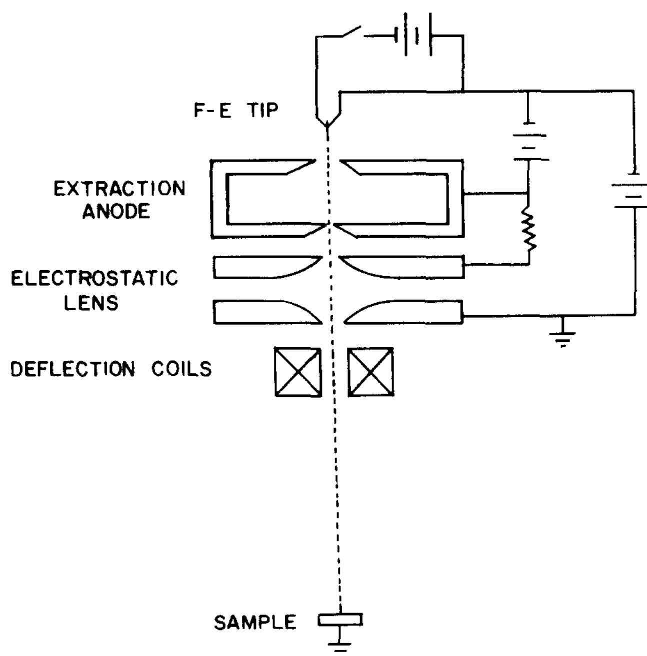

FIG. 12. Schematic diagram of a typical electron gun incorporating a field emission source.

Downloaded 05 Apr 2007 to 128.104.198.190. Redistribution subject to AIP license or copyright, see http://rsi.aip.org/rsi/copyright.jsp

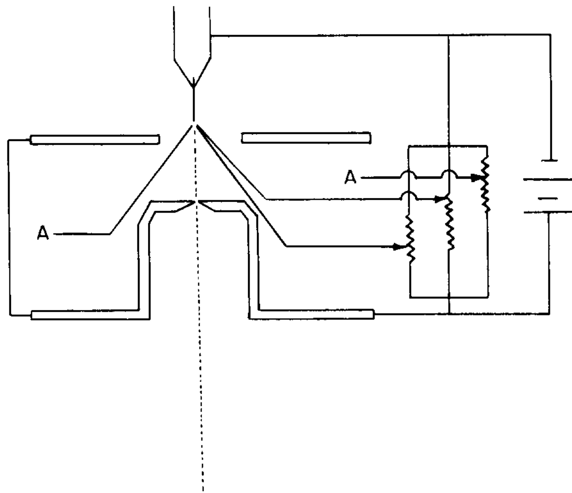

FIG. 13. Schematic diagram of extraction anode for a field emission gun that can be operated at low extraction potentials. Three tips opposing the field emitter act as extraction anodes. The potential on each is independently adjustable (Ref. 28).

passes through the opening in the extraction anode and is then focused by the lens system. The high kinetic energies imparted to the emitted electrons by the extraction anode present no difficulties in high-energy applications, where the electrons are usually further accelerated. For low-energy applications, the electrons must be decelerated with an appropriate lens system. The deceleration process tends to spread the electron beam spatially, because the beam is neither perfectly chromatic nor perfectly parallel, and because all lens systems have aberrations. In general, the relative distortion a lens introduces depends on how strongly it must interact with the beam. The extraction potential can in principle be reduced by decreasing the separation between the tip and the extraction anode. Because of geometric factors, however, the separation between a flat-plate anode and a tip cannot be reduced indefinitely, because as one approaches the plane of the anode at the aperture, the anode can no longer be approximated by a large, flat conducting surface and it ceases to generate enough electric field strength at the tip to produce field emission. We have recently developed an anode configuration[28] that circumvents this difficulty and allows field emission at anode potentials as low as 150 V, and perhaps lower. A schematic diagram of the anode design is shown in Fig. 13. Three field emission tips positioned opposite the cathode tip serve as the anode. The potential on each tip is separately adjustable, allowing for beam steering and correction for anode tip misalignment. Currents as large as 1 nA at 150 eV have been routinely achieved. The beam size is less than 5 μm at a focal distance of 10 cm. The field emission gun is easily tunable over a wide range of energies with no beam motion or loss of response.[28] The beam can be rastered, making scanning LEED and scanning low-energy electron microscopy possible.

B. Detectors

Signal detection in LEED requires the measurement of an energy-and-angle-resolved current at a fixed energy E_p, where E_p may be as high as 1000 eV. The detector must be capable of (1) energy resolution, i.e., the separation of those electrons at or very near E_p from the inelastically scattered electrons, and (2) angular resolution, i.e., the ability to separate the current in one diffracted beam from all the others and to measure the angular distribution of current in one beam. Two types of detectors are in common use, a Faraday cup that is mechanically driven and a set of hemispherical grids with a fluorescent screen. Neither scheme, in its simplest form, provides any gain. The most common detector is the fluorescent screen with a set of nested grids, shown schematically in Fig. 3. The inner grid is operated at the same potential as the sample, to provide a field-free region around the sample. The next grid (or two grids) is set at a negative bias to filter inelastically scattered electrons. The difficulties with this arrangement have already been discussed. The outermost grid is again operated at ground potential but is not needed for dc LEED operation. (If no intensities are to be measured, actually only two grids are required.) The fluorescent screen is operated at several kV positive potential to give the electrons sufficient energy to excite the phosphor. The major advantage of this detector is that it provides a visual display of essentially all the back-diffracted beams, making a rapid determination of the size and shape of the surface or overlayer unit mesh a possibility. On the other hand, the ability to give a visual display makes the fluorescent screen an inelegant detector from the point of view of signal processing. In many applications beam currents must be measured. Because the fluorescent screen changes an electron signal to an optical signal, a reconversion to an electron signal is required. The efficiency of phosphors in converting electrons to photons depends, among other factors, on the phosphor particle size, the size distribution, and the thickness of the phosphor coating. Measurements on several fluorescent screens[29] indicate that the best resolution is obtained from a thin layer of fine phosphor particles, with the average layer thickness exceeding the mean particle diameter. However, the conversion efficiency decreases as the particle size decreases. Hence, for optimum resolution, uniformity, and efficiency, a distribution of particle sizes with a layer thickness equal to the size of the largest particles is most desirable.[29]

Intensities in typical intensity versus energy profiles vary over three orders of magnitude, requiring a similar dynamic range for the fluorescent screen/detector combination. The response of a phosphor screen can be assumed to be linear over the ranges of beam currents used in LEED.[30] However, the dynamic range of the phosphor generally does not match that of detectors used to measure the optical intensity in a diffraction spot. Maxima in intensity versus energy profiles for typical incident-beam currents may thus saturate the detector. If the incident-beam current is reduced, the minima in intensity versus energy profiles become buried in fluorescent-screen noise. A fluorescent screen is therefore not ideal for measuring beam intensities quantitatively. In some applications, absolute intensities are not required. For example, angular distributions are independent of beam current as long as the phosphor and the detector are not saturated. For such measurements, the fluorescent screen represents a detector with a very good response. Because the

Downloaded 05 Apr 2007 to 128.104.198.190. Redistribution subject to AIP license or copyright, see http://rsi.aip.org/rsi/copyright.jsp

average phosphor particle size is typically of the order of micrometers, the phosphor acts like a detector with a continuously movable, several-μm-wide aperture, which is so small that it contributes essentially nothing to the total instrument response. Of course, this optical signal must still be converted into electrons, and thus the aperture width of the light-sensitive detector must be included in the instrument response. The dynamic range must be high for this type of measurement.

An additional negative aspect of most standard fluorescent screens is that they are viewed in reflection, i.e., past the sample and through the grids. Aside from the fact that the sample blocks part of the field of view and that the grids cause a loss of more than half the light intensity from the screen because of their limited transmission (each grid has typically 0.8 to 0.9 transmission), viewing in reflection generally requires the detector to be 20 to 30 cm from the screen. This causes a significant loss of intensity. Transparent fluorescent screens (glass coated with SnO_2 and phosphor) have been used to avoid these problems. A light-sensitive detector can then be placed directly behind the screen.[31]

Spot telephotometers have commonly been used for recording the diffracted-beam intensity from fluorescent screens. It is difficult to follow the motion of diffraction spots on the screen with a photometer, and used in the dc mode, it lacks sensitivity. As a result, other methods of measuring the brightness of the fluorescent screen have been developed. To improve the sensitivity, Schrott *et al.*[32] have used a photodiode and synchronous detection, modulating the suppressor grid at 100 Hz. Background light is thus effectively removed. Stair *et al.*[33] recorded intensities by photographing the fluorescent screen at various diffraction conditions, using high-speed 35-mm film. In this way the intensities of all reflections are obtained at the same time under identical conditions, a method far preferable, in terms of data reliability, to measuring the intensity versus energy profiles sequentially. The film is subsequently scanned mechanically and digitized using a computerized microdensitometer. A computer program locates the diffracted beams and provides an integrated intensity for each reflection at each incident-beam energy. The time to develop and digitize the film is long, resulting in considerable delay between a measurement and the availability of the results of this measurement. A modification of the scanning procedure uses a vidicon camera interfaced to a minicomputer.[34] This reduces the delay time between measurement and availability of the results to about a day.

Photographing the screen leads to a reduction in total measurement time by introducing parallel detection, rather than the serial detection used in a telephotometer, but introduces no detector gain. A reduction in total exposure of one or two orders of magnitude (from 10^{16} electrons/mm^2 to 10^{14} electrons/mm^2 for a set of intensity versus energy curves for all observable beams) is achieved because of the parallel detection. However, whether obtained simultaneously or sequentially, measurements of an intensity for any one reflection still require the same incident-beam current and measurement time to achieve the same S/N ratio. Hence incident-beam currents must be of the same order of magnitude as for photometers in order to achieve a net gain in time. The use of photography can be eliminated and the total sensitivity increased by using a vidicon camera to view the fluorescent screen directly.[17,35,36] Lang *et al.*[36] describe a computerized system designed to measure intensity versus energy profiles as efficiently as possible. In a direct application, a vidicon can only measure diffracted-beam profiles sequentially, but used in this manner, it is possible to make real-time measurements. Despite the serial detection, the greater sensitivity of the vidicon compared to film gives about the same overall measurement time. For parallel detection, Lang *et al.*[36] introduced the use of a videorecorder to replace the film, decreasing the total measurement time for all observable reflections by about two orders of magnitude. Real-time measurements are, of course, not possible using the videorecorder.

Our system[17] is optimized for angular-profile measurements. Part of the image on the LEED screen is focused onto the sensitive element of a commercial vidicon tube equipped with an image intensifier. The detector is rastered over 500 channels per track and the signal is digitized at a rate of 1 conversion per 64 μs. The intensity distribution in one track is accumulated into a 500-channel memory array, with simultaneous subtraction of background light stored previously in a second array. This background light measurement is made, for example, by biasing the electron gun so that the beam cannot emerge or by turning off the voltage on the phosphor screen. The height of the track as well as the magnification of the optical system can be adjusted, effectively allowing changes in the detector dimensions relative to the intensity distribution on the screen. The contributions of the vidicon detector and lens to the instrument response can be defined in terms of an optical transfer function, which represents the response of an optical system to an object whose intensity varies sinusoidally in space.[37] The modulus of the optical transfer function, the modulation transfer function (MTF), is analogous to the instrument response function of a diffraction system. The resolution of the vidicon is 15 lines/mm at 50% MTF. This translates into a FWHM of the point spread function, which is the image the vidicon forms of a point source, of $\sim 30\,\mu$m. For the geometry of our system, this corresponds to a contribution to the minimum angle of resolution $\vartheta_{\text{vidicon}} = 0.025°$ at the center of the screen, negligible, for all intents, compared to the total minimum angle of resolution $0.2° < \vartheta_{\min} < 0.5°$. The contribution of the lens is of a similar magnitude, while that of the fluorescent screen is even less. Thus this type of detector scheme is excellent from the point of view of resolving power, although, as has been noted, the fact that grids are used affects the sensitivity and achievable S/N ratios.

The addition of a channel electron multiplier array[38] to the detector improves the sensitivity by introducing gain into the detector, but decreases the resolving power. The mean gain of a chevron (dual) channel plate array is of the order of 10^6. Thus a reduction in primary-beam current of 10^6 gives in principle the same S/N at the same measurement times. Because of the finite channel width, however, the use of channel plates causes a spatial broadening of the input signal. For chevron arrays this broadening is accentuated

Downloaded 05 Apr 2007 to 128.104.198.190. Redistribution subject to AIP license or copyright, see http://rsi.aip.org/rsi/copyright.jsp

because the signal coming into one channel in the first plate gets spread into several channels in the second. For a typical channel size of 25 μm, this results in a FWHM of the point spread function of about 75–100 μm, at least double that of the vidicon/optics/fluorescent-screen combination. If the resolving power is of no concern (e.g., in intensity versus energy profiles, where an integral over the diffraction spot is in any case taken), this combination represents an excellent detector scheme. In angular-profile measurements the limited resolving power that results with this detector becomes important. Although the detector response can, of course, be deconvoluted from the measured intensity distribution, it is clear that the increased sensitivity of channel plates brings with it a reduction of ultimate spatial resolution.

Because channel electron multiplier arrays are usually flat, the distortion introduced in beams entering the plates at angles away from the normal to the plates must be taken into account.

The sensitivity of the detector can be further increased by replacing the fluorescent screen with a position-sensitive pulse detector. With a fluorescent screen biased at a typical energy of 5 keV, the minimum measurable current (using a vidicon) is estimated to be 1000 pulses/s. A position-sensitive detector can measure individual pulses. The first such detector that was constructed for LEED[39] consists of a resistive-anode encoder (RAE) preceded by a chevron channel electron multiplier array. An RAE is a continuous resistive film that acts as a current divider for an incoming pulse of electrons, thus determining its spatial position. For example, for a square film of dimension $d \times d$, with current pickups at the corners, the position of a pulse is given by

$$\frac{y}{d} = \frac{i_{0,d} + i_{d,d}}{i_{00} + i_{d,0} + i_{0,d} + i_{d,d}}, \tag{12}$$

where $0,d$ are the coordinates of the pickups. A similar expression holds for the position x. Thus measuring the individual pulse heights at the pickups determines the position of the pulse impact. Although this type of detector determines the centroid of the arriving pulse, the spatial resolution is nevertheless not good. The spatial resolution is determined by the extent to which the thermal noise perturbs the pulse currents. Thus, a trade-off between detector area and maximum allowable thermal noise occurs. For a 75-mm-square RAE, the lateral resolution is estimated to be between 300 and 400 μm.[39,40] The RAE can accommodate 50-kHz pulse arrival rates. Data rates are therefore limited by the individual-channel dead time in the chevron channel plates and not by the RAE.

The difficulty with loss of lateral resolution due to thermal noise can possibly be avoided by using a wedge-and-strip anode detector.[41,42] The wedge-and-strip anode is a position-sensitive pulse counting detector that was described some time ago.[41] Recently new anode geometries have been developed, and the characteristics of such devices investigated.[42] The principle of operation, like that of the RAE, is the division of the charge in a pulse incident on the anode among several output terminals, but the wedge and strip is a conductive sheet rather than a resistor. Figure 14 shows a wedge-and-strip anode schematically. The equations for the

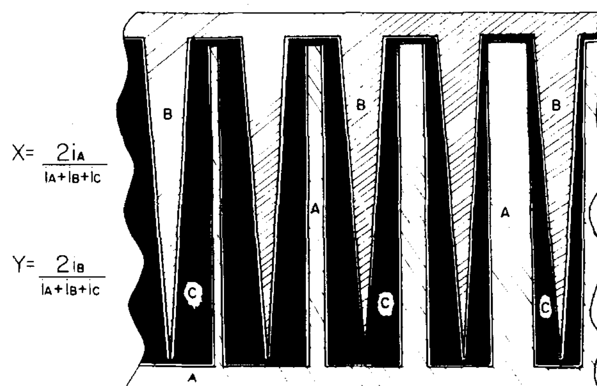

FIG. 14. Schematic diagram of a wedge-and-strip anode. A, B, and C are three sets of conductors. The positions x and y are given in terms of the currents to collectors A, B, and C as indicated by the equations.

determination of the x and y positions of the pulse centroid are

$$x = 2i_A/(i_A + i_B + i_C)$$
$$y = 2i_B/(i_A + i_B + i_C), \tag{13}$$

where i_A, i_B, and i_C are the electrical charge signals collected by the three groups of conductors shown. Note that the dimensions of the respective conductors change away from the center of the anode. It is this feature that makes the device position sensitive.[41,42] The spatial resolution of the device is limited by the uncertainty in determining the position of the centroid of the incident pulse, and this is a function of the conductor size and density. Reference 42 shows spatial resolution of better than 100 μm for a 3.5×3.5-cm anode, and better than 50 μm for a 2.5×2.5-cm anode, with conductor dimensions in both of the order of 1 mm. The spatial resolution is constant over the entire detecting area. Amplifier input noise introduced by the interelectrode capacitance of the array is the primary source of centroid-position uncertainty and thus loss of spatial resolution. As in the case of the RAE, the anode is the component that limits the resolving power. The maximum pulse rate that can be handled by the anode is similar to that of the RAE, of the order of 10^4 to 10^5 Hz.[42] Thus the channel plates limit the ultimate sensitivity of a grid/channel plate/position-sensitive anode detector.

The ultimate presently attainable sensitivity and angular resolution are provided by a Faraday cup detector equipped with a channel electron multiplier. With this arrangement individual pulses can be counted, and by making the aperture of the detector arbitrarily small, any degree of angular resolution can be obtained. Such detectors are in common use in a variety of spectroscopic techniques, including LEED. Gronwald and Henzler[43] have described a Faraday cup detector that includes deflection plates in front of the aperture so that the beam profile can be measured without mechanical motion of the detector. Some Faraday cup detector designs contain no retarding grids but nevertheless provide much better energy resolution than is obtained with detectors incorporating grids. Such detectors consist of a deep cup in close proximity to but electrically isolated from an aperture plate. The diameter of the cup is several times the diameter of the aperture, and the depth of the cup is

Downloaded 05 Apr 2007 to 128.104.198.190. Redistribution subject to AIP license or copyright, see http://rsi.aip.org/rsi/copyright.jsp

several times its diameter. The cup is biased negatively to within 1 to 2 eV of the energy of the elastically scattered electrons. This detector provides excellent energy resolution (of the order of the thermal spread in the incident beam) without significant loss of secondary electrons from the cup. Because the field outside the aperture is negligible the angular distribution of electrons in the diffracted beam being measured is not disturbed. The advantage of good energy resolution is that inelastically scattered electrons can be eliminated to a much greater degree, making the background in angular-profile measurements less of a problem. Finally, a Faraday cup detector is the only means to measure analog signals quantitatively. Hence it is preferable for every LEED instrument to have two detectors, the Faraday cup for quantitative current and ultimate angular resolution measurements, and some form of position-sensitive detector for the rapid data acquisition required for accurate structural determination within the time or electron dose constraints of a typical surface crystallography experiment.

C. Goniometers

The function of a goniometer is to position the crystal accurately with respect to the incident beam of electrons. As mentioned, the importance of such accuracy depends on the experiment being performed. For intensity versus energy profiles, it is critical that the absolute angle be well known and that the repeatability of setting these angles be excellent. For angular-profile measurements, absolute angles are not important. Standard UHV manipulators are commonly used. Although they are not very precise, it is possible to set normal incidence of the beam by comparison of intensities in symmetrically positioned beams. Deviations from normal incidence are then usually made only in one plane, the colatitude. More precise goniometers also include an azimuthal motion.

Goniometers for special purposes have been built. An exceedingly precise one[44] was constructed to perform automatically constant-momentum-transfer-averaging[45] of intensities. In this technique, the momentum transfer vector must remain constant as the angle of incidence and the scattering angle are changed. To provide this condition automatically, the goniometer is constructed to couple the motions of the Faraday cup and the crystal in colatitude. Uncoupling of the motions is also possible to permit arbitrary angles of incidence and diffraction.

For fine-beam or scanning LEED applications it is also necessary that the goniometer be stable against vibrations. For such applications, which will become possible in the near future, modified versions of manipulators used for scanning Auger spectroscopy or similar techniques can be used.

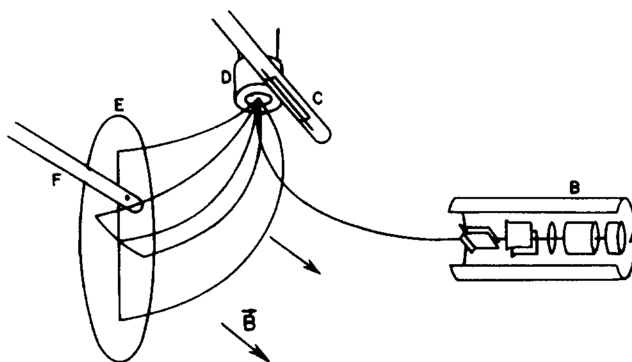

FIG. 16. Schematic diagram of the diffractometer of Dennis and Webb[25] using magnetic deflection through 180°. A: electron gun; B: magnetic shielding; C: probe for measuring beam intensity and profile; D: sample; E: fluorescent screen; F: Faraday cup detector.

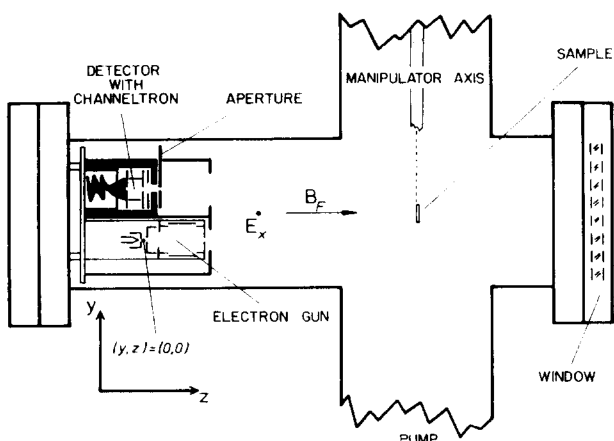

FIG. 15. Schematic diagram of the diffractometer of Wulfert and Henzler,[27] incorporating a magnetically focused gun.

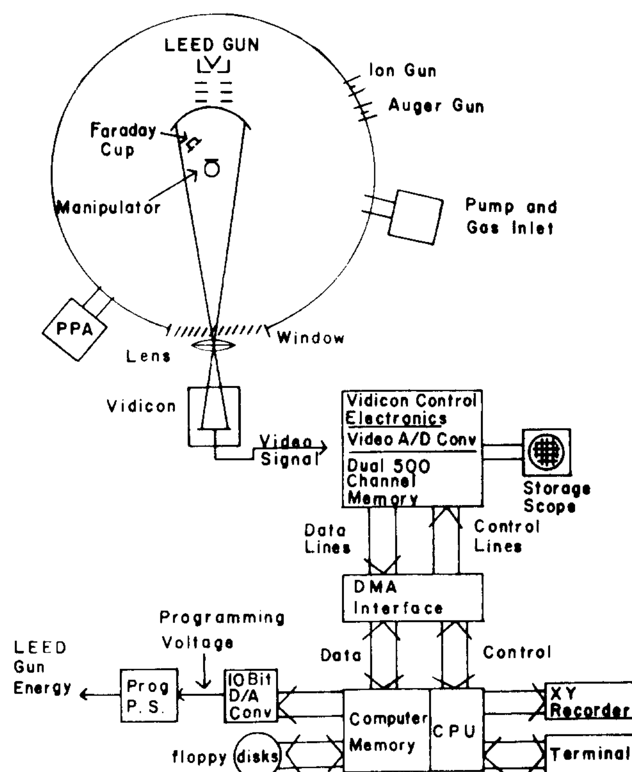

FIG. 17. Schematic diagram of a diffractometer using a vidicon camera as a detector (Ref. 17).

Downloaded 05 Apr 2007 to 128.104.198.190. Redistribution subject to AIP license or copyright, see http://rsi.aip.org/rsi/copyright.jsp

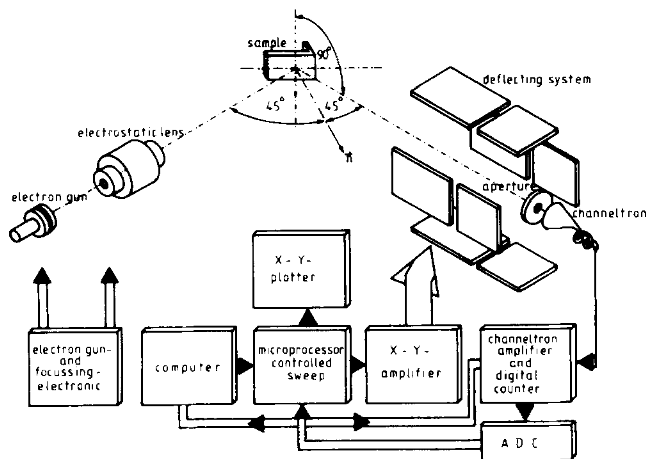

FIG. 18. Schematic diagram of the diffractometer of Gronwald and Henzler,[43] incorporating a Faraday cup detector with channeltron and deflection plates.

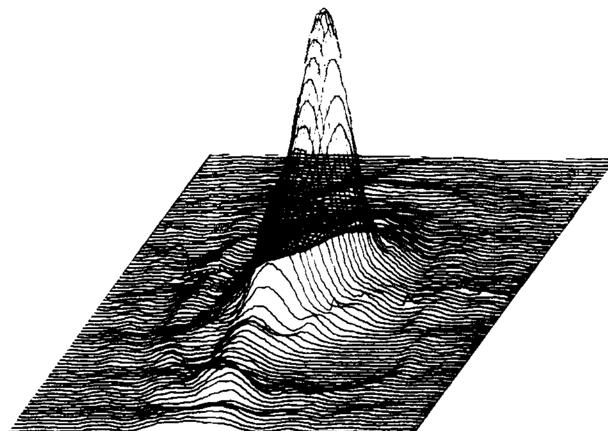

FIG. 19. Contour plot of a diffracted beam from Si(111) taken with the system of Fig. 18 (Ref. 43).

D. Complete systems

In the last three sections, the major components of a LEED diffractometer were discussed in detail. In this section several complete systems are shown schematically and the performance of some of them illustrated. The magnetic-deflection system of Dennis and Webb[25] is shown in Fig. 15. Wulfert's magnetically-focused-gun system[27] is shown in Fig. 16. The system of Welkie[17] incorporating a vidicon detector is shown in Fig. 17. In addition to the components already described, it includes computer-based data acquisition and instrument control. Results of angular profiles taken with this system[18] were shown in Fig. 7. The system of Gronwald and Henzler,[43] incorporating the Faraday cup detector with deflection plates and computer control, is shown in Fig. 18. An additional feature of this system is the operation at an angle of incidence of 45°. Operation at glancing angles makes possible an increase in instrument response[11,15] relative to operation at normal incidence. A detailed measurement of a LEED spot using this system is shown in Fig. 19. A prototype system incorporating a wedge-and-strip anode detector[22] is shown schematically in Fig. 20. Figure 21 shows a comparison of the instrument response of typical commercial systems and the newest high-resolving-power diffractometers.

III. COMPARISON TO OTHER TECHNIQUES GIVING SURFACE CRYSTALLOGRAPHIC INFORMATION

A number of other techniques exist that provide surface crystallographic information. Each of them has its own strengths and weaknesses, but none is as well developed for surface crystallography as is LEED. Ions, x rays, and fast electrons have been used. Low-energy ions are used in ion-scattering spectroscopy (ISS), where the backscattered flux of ~ 1000-eV ions in a particular direction is measured.[46] Structural information can be obtained by using the fact that

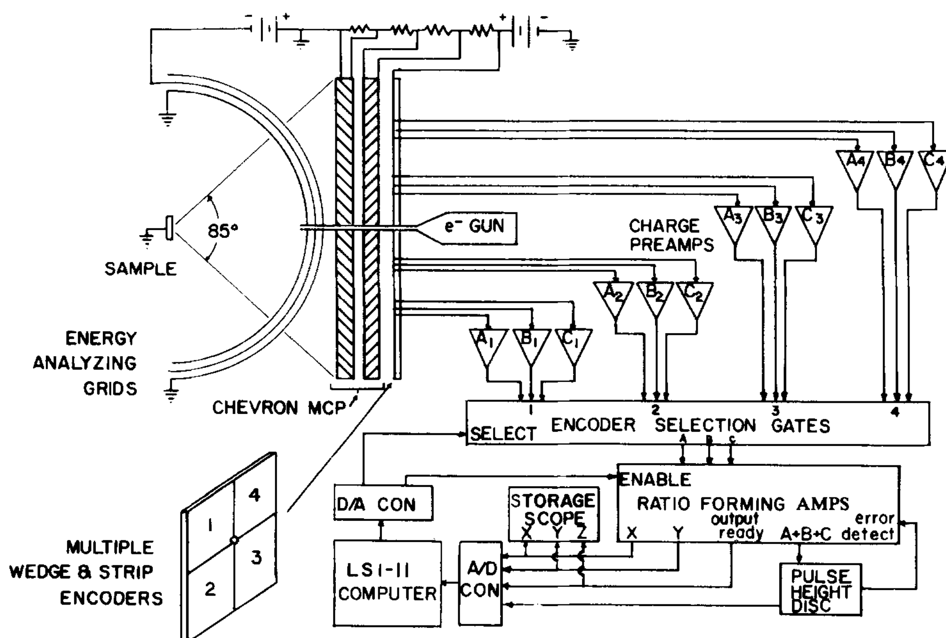

FIG. 20. Schematic diagram of a design for a diffractometer with a chevron multichannel plate/wedge-and-strip-anode detector.

Downloaded 05 Apr 2007 to 128.104.198.190. Redistribution subject to AIP license or copyright, see http://rsi.aip.org/rsi/copyright.jsp

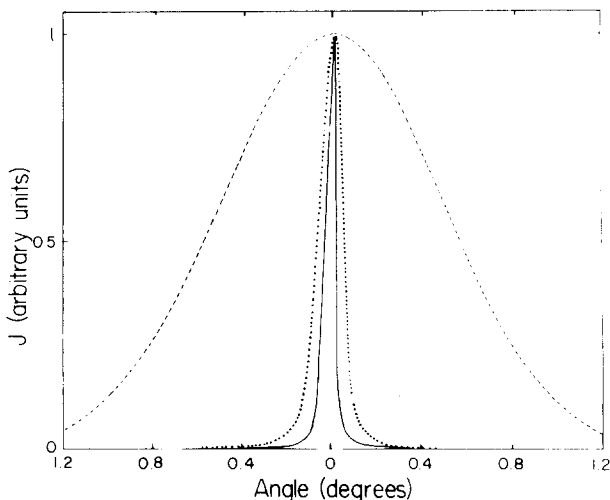

FIG. 21. Relative angular widths of instrument response functions for three LEED diffractometers. Dashed curve, typical commercial system; dotted curve, system with magnetically focused gun and Faraday cup[27]; solid curve, system with field emission gun and knife-edge Faraday cup.[28]

an atom in the path of the incoming ions will shadow other atoms behind it. Thus it is possible to determine, for example, for an adsorbed overlayer on an fcc (110) surface, whether the adsorbed atoms sit in the troughs or on top, by comparing the strength of the overlayer scattering in two perpendicular directions. Unfortunately, the cross sections for scattering of ions at these low energies are not well known and, as a result, it is difficult to extract accurate values for equilibrium atom positions from such measurements. Phase transition or disordering measurements are also possible with ISS, by observing a decay of scattered flux in particular directions as the temperature is raised.[47]

Ions at energies of the order of 2 MeV can be used to perform Rutherford ion backscattering spectroscopy (RIBS) of surfaces. An excellent review comparing the capabilities of RIBS and LEED has been written by Feldman.[48] The principle of RIBS is the same as that of low-energy ion scattering, i.e., the shadowing of atoms in a line behind the surface atom, but the cross sections are much more precisely known. In some cases it should be possible to extract structural information using RIBS that is as accurate as or more accurate than LEED. For example, the technique is quite sensitive to lateral positions. The principal difference between diffraction and ion scattering is the distance parameter for order that is probed by the technique. LEED is sensitive to order over large distances, while ion scattering senses the local position of surface atoms relative to their bulk position. This implies that RIBS is not sensitive to defects. Additionally, ion scattering is "mass dispersive,"[48] i.e., it can separately determine the atomic coordinates of adsorbate and substrate atoms. A difficulty with the technique is that the shadow cone produced by an atom is so narrow that even small uncertainties in vibrational amplitudes can produce large uncertainties in position determinations. This problem can in part be surmounted by operation at medium energies, e.g., ~ 100 keV. This improves the surface sensitivity and widens the shadow cone. However, cross sections for scattering are not as well known in this energy range.

Several techniques also exist that provide surface structural information by using fast electrons. The major one is reflection high-energy electron diffraction (RHEED), with or without subsequent imaging. In RHEED, a high-energy electron beam (5–100 keV) is incident on the sample at a grazing angle, sufficiently small so that the penetration of the beam is limited and a reasonable fraction of the diffracted intensity comes from the surface layer. Transmission electron microscopes (TEM) with improved vacuum have recently been used in this mode to perform surface crystallography experiments.[49] Both diffraction pictures[49,50] and subsequent images[49] have been obtained. This method appears to be quite powerful because of the better control on beam size and divergence at the high energies. The major disadvantages at this stage appear to be the lack of flexibility in sample positioning and in inclusion of other surface analysis techniques, and the extreme foreshortening of features in the image that results from the use of very small angles of incidence (of the order of 1°). The fine beam size (tens of Å) makes possible the observation of individual structural features of that order of magnitude. For example, individual steps have been observed.[51] As a consequence it is, of course, more difficult to observe average effects over a surface, such as average size distributions of growing islands or average step densities.

Conventionally, RHEED is associated with lower-energy beams than TEM and no imaging, and is done in an ultrahigh vacuum system along with several other surface analysis techniques. In this mode, RHEED has been practiced for a number of years with some early quite interesting results.[52] RHEED has been used to study crystallographic phenomena at high temperatures, such as epitaxial growth. LEED measurements at angles far from normal will, in fact, allow higher-temperature observations than RHEED because the Debye–Waller factor can be kept smaller. The major advantage of RHEED is the much higher resolving power in the plane of incidence, a consequence of the grazing angle of incidence and the resulting nearly tangential cut of the Ewald sphere across a rod.[53] This geometry leads to elongated diffraction features, or "streaks." The length of these streaks represents the main uncertainty in the interpretation of RHEED. The existence of streaks has been variously ascribed to a very good surface, a poor surface, a poor instrument, and thermal diffuse scattering. It can easily be demonstrated that the instrument response of even the worst RHEED systems cannot cause the streaks that are observed. Furthermore, a good surface does not produce streaks but spots.[51,54,55] The most likely contributions to streak length are defects, such as steps or long-range curvature of the surface.[54,55] At present, it is still considerably more difficult to interpret RHEED profiles than LEED profiles, although the prospect of much increased resolving power provides the motivation for rapid progress in our understanding of the technique.[53,55]

X-ray diffraction at grazing incidence has recently been used to study surfaces.[56] This technique is insufficiently developed to evaluate its strengths and weaknesses. It appears to be quite powerful because multiple-scattering effects are probably much less important. On the other hand, low beam

Downloaded 05 Apr 2007 to 128.104.198.190. Redistribution subject to AIP license or copyright, see http://rsi.aip.org/rsi/copyright.jsp

intensity could cause signal-to-noise problems. Additionally there are difficulties associated with glancing incidence, both in limiting observable diffraction space, and in causing streaks, as discussed above.

A final technique that should be mentioned is low-energy mirror microscopy. In this technique, a high-energy beam is decelerated just before reaching the surface, and reaccelerated after diffraction by the surface. A diffracted beam, after acceleration, is then imaged in the traditional way.[57] The interpretation of mirror microscopy images is quite complicated, and to our knowledge, no crystallography experiments have been performed on single-crystal surfaces prepared in ultrahigh vacuum.

IV. CONCLUSIONS

Low-energy electron diffraction is the most well-developed technique for surface crystallography studies. In this review, we have discussed the types of measurements important in surface crystallography and have described the major advances in instrumentation that have been made in recent years. It is apparent that there are still instrumental limitations, especially in detectors. It is expected that further improvements in detector or electron beam technology, when they occur, will be incorporated readily into LEED instrumentation. In particular, the progress that has been made in instrumentation for high-energy electron beam techniques will influence the development of electron sources at low energies. Especially, one can look forward to imaging at low energies, although it is unlikely that beam optics and detector sensitivities at low energies can ever be developed as well as is the present standard in high-energy electron microscopy.

ACKNOWLEDGMENTS

We thank D. Savage and T.-M. Lu for useful discussions and M. Henzler for supplying a dissertation and preprints prior to publication. NSF has supported our LEED instrumentation development under Grant No. DMR 72-03249 and DMR 82-07255.

[1]C. J. Davisson and L. H. Germer, Phys. Rev. **30**, 705 (1927).
[2]W. T. Sproull, Rev. Sci. Instrum. **4**, 193 (1933).
[3]W. Ehrenberg, Philos. Mag. **18**, 878 (1934).
[4]J. J. Lander, J. Morrison, and F. Unterwald, Rev. Sci. Instrum. **33**, 782 (1962).
[5]C. W. Caldwell, Rev. Sci. Instrum. **36**, 1500 (1965).
[6]R. L. Park and H. E. Farnsworth, Rev. Sci. Instrum. **35**, 1592 (1964).
[7]For a recent review, see M. G. Lagally, Appl. Surf. Sci. **13**, 260 (1982).
[8]For reviews, see (a) M. B. Webb and M. G. Lagally, Solid State Phys. **28**, 305 (1973); (b) J. B. Pendry, *Low-Energy Electron Diffraction* (Academic, New York, 1974); (c) J. A. Strozier, D. W. Jepsen, and F. Jona, in *Surface Physics of Materials*, edited by J. M. Blakely (Academic, New York, 1975); (d) M. A. van Hove and S. Y. Tong, *Surface Crystallography by LEED* (Springer, Berlin, 1979); (e) M. A. van Hove, in *The Nature of the Surface Chemical Bond*, edited by T. N. Rhodin and G. Ertl (North-Holland, Amsterdam, 1979).
[9]See, for example, W. W. Beeman, P. Kaesberg, J. W. Anderegg, and M. B. Webb, in *Handbuch der Physik*, edited by S. Flügge (Springer, Berlin, 1957), Vol. 32; (b) A. Guinier, *X-Ray Diffraction* (Freeman, San Francisco, 1963); (c) B. E. Warren, *X-Ray Diffraction* (Addison-Wesley, Reading, MA, 1969).
[10](a) M. Henzler, in *Electron Spectroscopy for Surface Analysis*, edited by H. Ibach (Springer, Berlin, 1977); (b) Appl. Surf. Sci. **11/12**, 450 (1982); (c) M. G. Lagally and D. G. Welkie, in *Advanced Techniques for Characterizing Microstructures*, edited by F. W. Wiffen and J. A. Spitznagel (The Metallurgical Society of AIME, Warrendale, PA, 1982); (d) M. G. Lagally, in *Chemistry and Physics of Solid Surfaces*, Vol. IV, edited by R. Vanselow, and R. Howe, *Springer Series in Chemical Physics* (Springer, Heidelberg, 1982), Vol. 20; (e) R. L. Park, J. Appl. Phys. **37**, 295 (1966); (f) J. E. Houston and R. L. Park, Surf. Sci. **21**, 209 (1970); **26**, 269 (1971); (g) S. C. Fain, Jr. and M. D. Chinn, J. Phys. (Paris) **38** Suppl. 10, C4-99 (1977); (h) P. J. Estrup and E. G. McRae, Surf. Sci. **25**, 1 (1971); (i) S. Semancik and P. J. Estrup, J. Vac. Sci. Technol. **18**, 541 (1981); (j) R. A. Barker and P. J. Estrup, J. Chem. Phys. **74**, 1442 (1981).
[11]R. L. Park, J. E. Houston, and D. G. Schreiner, Rev. Sci. Instrum. **42**, 60 (1971).
[12]T.-M. Lu and M. G. Lagally, Surf. Sci. **99**, 695 (1980).
[13]See, for example, K. R. Spangenberg, *Fundamentals of Electron Devices*, (McGraw-Hill, New York, 1957); R. L. Park, in *Experimental Methods in Catalytic Research*, edited by M. Dawson and C. A. Anderson (Academic, New York, 1976), Vol. III.
[14]For a lucid discussion of the proper interpretation of instrument response functions and "coherence widths" in LEED, see G. Comsa, Surf. Sci. **81**, 57 (1979).
[15]G.-C. Wang and M. G. Lagally, Surf. Sci. **81**, 69 (1979).
[16]T.-M. Lu, M. G. Lagally, and G.-C. Wang, Surf. Sci. **104**, L229 (1981).
[17]D. G. Welkie and M. G. Lagally, Appl. Surf. Sci. **3**, 272 (1979).
[18]H. M. Clearfield (unpublished).
[19]For reviews, see R. F. Wallis, in *Progress in Surface Science*, edited by S. G. Davison (Pergamon, New York, 1973), Vol. 4; M. G. Lagally, in *Surface Physics of Materials*, edited by J. M. Blakely (Academic, New York, 1975).
[20]Cliftronics, Model 406-S, Clifton, NJ.
[21]J. A. Martin and M. G. Lagally, J. Vac. Sci. Technol. **18**, 58 (1981).
[22]J. A. Martin (unpublished).
[23]W. N. Unertl (private communication).
[24]C. W. Tucker, Jr., Appl. Phys. Lett. **1**, 34 (1962).
[25]R. L. Dennis, Ph.D. dissertation, University of Wisconsin-Madison, 1972 (unpublished); R. L. Dennis and M. B. Webb, J. Vac. Sci. Technol. **10**, 192 (1973).
[26]P. I. Cohen, Ph.D. dissertation, University of Wisconsin-Madison, 1975 (unpublished); P. I. Cohen, J. Unguris, and M. B. Webb, Surf. Sci. **58**, 429 (1976).
[27]F.-W. Wulfert, Ph.D. dissertation, University of Hannover, 1982 (unpublished); Ref. 10b.
[28]J. A. Martin and M. G. Lagally, J. Vac. Sci. Technol. A **1**, 1210 (1983).
[29]K. G. Predko and M. P. Znachenok, J. Appl. Spectrosc. (USSR) **10**, 694 (1969); I. P. Csorba, RCA Rev. **30**, 36 (1969).
[30]A. Bril and F. A. Kröger, Phillips Tech. Rev. **12**, 120 (1950).
[31]L. de Bersuder, Rev. Sci. Instrum. **45**, 1569 (1972); P. A. Bennett and M. B. Webb (private communication).
[32]A. G. Schrott, M. D. Chinn, C. G. Shaw, and S. C. Fain, Jr., J. Vac. Sci. Technol. **21**, 101 (1982).
[33]P. C. Stair, T. J. Kaminska, L. L. Kesmodel, and G. A. Somorjai, Phys. Rev. B **11**, 623 (1975).
[34]D. C. Frost, K. A. R. Mitchell, F. R. Shepherd, and P. R. Watson, J. Vac. Sci. Technol. **13**, 1196 (1976); T. N. Tommet, G. B. Olszewski, P. A. Chadwick, and S. L. Bernasek, Rev. Sci. Instrum. **50**, 147 (1979).
[35]P. Heilman, E. Lang, K. Heinz, and K. Müller, Appl. Phys. **9**, 247 (1976).
[36]E. Lang, P. Heilman, G. Hanke, K. Heinz, and K. Müller, Appl. Phys. **19**, 287 (1979).
[37]R. L. Lamberts, G.-C. Higgins, and R. N. Wolfe, J. Opt. Soc. Am. **48**, 487 (1958); R. C. Lamberts, J. SMPTE **71**, 635 (1962).
[38]M. D. Chinn and S. C. Fain, J. Vac. Sci. Technol. **14**, 314 (1977).
[39]P. C. Stair, Rev. Sci. Instrum. **51**, 132 (1980).
[40]M. Lampton and F. Paresce, Rev. Sci. Instrum. **45**, 1098 (1974).
[41]H. O. Anger, Instrum. Soc. Am. Trans. **5**, 311 (1966).
[42]C. Martin, P. Jelinsky, M. Lampton, R. F. Malina, and H. O. Anger, Rev. Sci. Instrum. **52**, 1068 (1981).
[43]K. D. Gronwald and M. Henzler, Surf. Sci. **117**, 180 (1982).
[44]P. A. Bennett, Ph.D. dissertation, University of Wisconsin-Madison, 1980 (unpublished); P. A. Bennett and M. B. Webb, Surf. Sci. **104**, 74 (1981).
[45]Tran C. Ngoc, M. G. Lagally, and M. B. Webb, Surf. Sci. **35**, 117 (1973).
[46]W. Heiland, Appl. Surf. Sci. **13**, 282 (1982). This review contains a list of

Downloaded 05 Apr 2007 to 128.104.198.190. Redistribution subject to AIP license or copyright, see http://rsi.aip.org/rsi/copyright.jsp

additional reviews. W. Heiland and E. Taglauer, in *Methods of Experimental Physics: Surfaces* edited by R. L. Park and M. G. Lagally (in press).
[47]S. H. Overbury, W. Heiland, D. M. Zehner, S. Datz, and R. S. Thoe, Surf. Sci. **109**, 239 (1981).
[48]L. C. Feldman, Surf. Sci. **13**, 211 (1982).
[49]N. Osakabe, Y. Tanashiro, K. Yagi, and G. Honjo, Surf. Sci. **97**, 393 (1980); **102**, 424 (1981); N. Osakabe, K. Yagi, and G. Honjo, Jpn. J. Appl. Phys. **19**, L309 (1980); P. S. Turner and J. M. Cowley, Ultramicroscopy **6**, 125 (1981); J. M. Cowley, J. L. Albain, G. G. Hembree, P. E. Hojlund-Nielsen, F. A. Koch, J. D. Landry, and H. Schumann, Rev. Sci. Instrum. **46**, 826 (1975). For additional references and a brief discussion, see J. A. Venables, in *Chemistry and Physics of Solid Surfaces*, Vol. IV, edited by R. Vanselow and R. Howe, *Springer Series in Chemical Physics* (Springer, Heidelberg, 1982), Vol. 20. See also papers in Ultramicroscopy **8** (1983).
[50]S. Ino, Jpn. J. Appl. Phys. **26**, 891 (1977).
[51]Osakabe *et al.*, Ref. 49.
[52]K. Matysik, Surf. Sci. **46**, 457 (1974); J. Appl. Phys. **47**, 3826 (1976).
[53]J. M. Van Hove, P. Pukite, P. I. Cohen, and C. S. Lent, J. Vac. Sci. Technol. A **1**, 609 (1983).
[54]J. F. Menadue, Acta Cryst. A **28**, 1 (1972).
[55]J. M. Van Hove, C. S. Lent, P. R. Pukite, and P. I. Cohen, J. Vac. Sci. Technol. B **1**, 741 (1983).
[56]W. C. Marra, P. E. Eisenberger, and A. Y. Cho, J. Appl. Phys. **50**, 6927 (1979); W. C. Marra, P. H. Fuoss, and P. E. Eisenberger, Phys. Rev. Lett. **49**, 1169 (1982); I. K. Robinson, Phys. Rev. Lett. **50**, 1145 (1983).
[57]A. Bok, in *Modern Diffraction and Imaging Techniques in Material Science*, edited by S. Amelinckx, R. Gevers, G. Remaut, and J. Van Landuyt (North-Holland, Amsterdam, 1970).

PRICING AND ORDERING INFORMATION FOR REVIEW-ARTICLE REPRINTS

PRICES: $5.00; $4.50 each for bulk orders of ten or more copies of the same article sent to one address. Delivery is via surface mail. Airmail delivery available at the following surcharge: $2.50 for the first copy plus $1.00 for each additional copy sent to one address. *Reprint orders must be prepaid.*

ORDERS: Please specify REVIEW OF SCIENTIFIC INSTRUMENTS REVIEWS and give the article title, authors, month, and year of publication, and the page number of the article's title page. Send orders accompanied by payment in full (make checks payable to American Institute of Physics) to: *Current Physics Reprints, American Institute of Physics, 335 East 45th Street, New York, NY 10017.*

Downloaded 05 Apr 2007 to 128.104.198.190. Redistribution subject to AIP license or copyright, see http://rsi.aip.org/rsi/copyright.jsp